Journal of Science and Transport Technology
Journal homepage: https://jstt.vn/index.php/en

UNIVERSITY OF TRANSPORT TECHNOLOGY

Electro-Mechanical Receptance for Cracked Piezoelectric FGM Beam

Nguyen Ngoc Huyen[1*], Luu Quynh Huong[1], Nguyen Tien Khiem[2*]
[1]Thuyloi University, 175 Tay Son, Kim Lien Ward, Hanoi, Vietnam
[2]HUTECH University, 475A Dien Bien Phu, Thanh My Tay Ward, Ho Chi Minh City, Vietnam

Article info
Type of article:
Original research paper

DOI:
https://doi.org/10.58845/jstt.utt.2026.en.6.4.144-160

***Corresponding authors:**
Email address:
nnhuyen@tlu.edu.vn
nt.khiem55@hutech.edu.vn

Received: 13/12/2025
Received in Revised Form: 14/05/2026
Accepted: 26/05/2026

Abstract: In this study, the concept of electro-mechanical receptance (EMR) is introduced for cracked functionally graded beams integrated with a piezoelectric layer. A double-spring model is employed to represent a transverse edge crack in functionally graded Timoshenko beams subjected to harmonic point excitation. The electrical response of the piezoelectric layer is then derived in an analytical form, enabling the formulation of EMR for such beam systems. The proposed EMR is subsequently examined with respect to material properties and crack parameters, including location and depth, and its applicability for crack detection is discussed.

Keywords: Cracked beams; Functionally Graded Materials (FGM); Piezoelectric layer; Receptance.

1. Introduction

Functional graded material (FGM) is an advanced composite material that can eliminate numerous drawbacks of the traditional laminated composites and increase their resistance to both mechanical and thermal loads. The fundamentals of modelling and analysis of structures made of FGM were provided in [1, 2]. Recently, the problems of vibration in intact FGM structures [3–5] and cracked ones [6–8] have been reported. Also, though some procedures were proposed for crack identification in functionally graded beams and published in [9–11], smart materials such as piezoelectric ones have been employed recently for crack detection of functionally graded beam structures only in [12].

Piezoelectric material has found an effective application in structural health monitoring (SHM) [13–16] where it is usually employed for actuating the structures of interest and sensing their response behavior. The use of piezoelectric material as both actuator and sensor in SHM leads to developing a technique called electro-mechanical impedance (EMI) method [17–19] that was then efficiently applied for crack detection in engineering structures [20–24]. Nevertheless, the EMI technique still has some drawbacks such as (a) it works only in the high frequency range, where measured signals are often polluted with noise; (b) activity zone of the impedance transducer is limited to its size and (c) damage signature contained in the measured impedance signals is usually small and difficult to apprehend. Therefore, aimed at avoiding the drawbacks of EMI technique, some authors have proposed to use mechanical load instead of piezoelectric actuator employed in the EMI method [25–27].

Namely, Sumant and Maiti [26] used a pair of piezoelectric patches as sensors attached to the top and bottom surfaces of a beam at a position to measure electric voltage produced in the patches in response to a concentrated static load for detecting a crack in the beam. The authors observed that the measured voltage variation increases with increasing crack depth, while it decreases as the distance between the crack and the sensor patch becomes larger. The voltage in the patches was dropped if the distance between the crack and patches positions is less than the beam thickness. The voltage drops allow detecting a small crack of 3% depth with an error less than 5% in crack localization and 10% in crack depth estimation.

Used the same approach as applied in [26], Roy et al. [25] examined a crack detection procedure by employing piezoelectric patch of various length included also a piezoelectric strip of the same length as beam. A conclusion made by the authors of [25] is that the patch of whole beam length makes the crack detection procedure much easier, especially in detection of multiple cracks. Indeed, it was demonstrated in [27] that a piezoelectric layer employed as a distributed sensor in combination with a controlled moving load allows for a closed solution to the crack identification problem in beam-structures. The important finding of the latter study is that by using mechanical dynamic load instead of electrical one the crack detection can be accomplished in the lowest frequency range. This is a significant improvement in using the EMI method.

Thus, continuing the idea of replacing electrical excitation with mechanical load and lowering down the working frequency range of EMI technique, a new concept called EMR was proposed and studied in [28] for cracked homogeneous beam with piezoelectric layer. This concept is extended in present study for cracked functionally graded beam and its sensitivity to crack is examined along the material gradation index.

2. Modelling of cracked piezoelectric functionally graded beams

Consider an FGM beam of length L, cross sectional area $A_b = b \times h_b$, bonded with a piezoelectric layer (Fig. 1). Material distribution along thickness direction of the host beam is assumed according to the power law represented by [1]

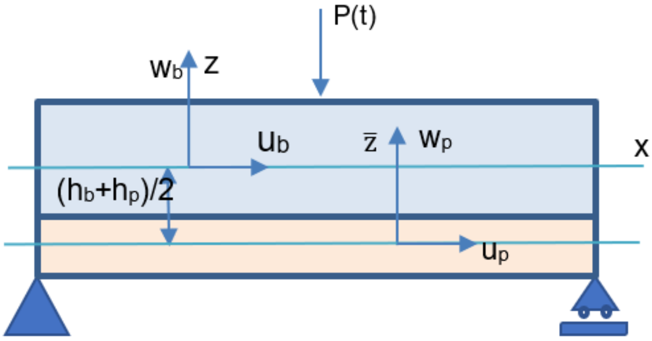

Fig. 1. FGM beam element with piezoelectric layer

$$\Re(z) = \Re_b + (\Re_t - \Re_b)\left(\frac{z}{h} + 0.5\right)^n; \quad -\frac{h_b}{2} \le z \le \frac{h_b}{2}, \qquad (1)$$

where $\Re_b, \Re_t$ denote the Young's modulus, shear modulus, and mass density E, G, ρ at bottom and on the top of the beam respectively. The parameter n represents the material gradient index and z is the coordinate measured along the beam thickness from the mid-plane. Based on the Timoshenko beam theory, the governing constitutive relations are expressed as [8]

$$\begin{aligned} & w(x,z,t) = w_0(x,t); \\ & u(x,z,t) = u_0(x,t) - \theta(x,t)(z - h_0); \\ & \sigma_x = E(z)\varepsilon_x; \\ & \tau_{xz} = \kappa\gamma_{xz}G(z); \\ & \varepsilon_x = \frac{\partial u_0}{\partial x} - \frac{\partial \theta}{\partial x}(z - h_0); \\ & \gamma_{xz} = \frac{\partial w_0}{\partial x} - \theta, \end{aligned} \qquad (2)$$

where $u_0(x,t)$, $w_0(x,t)$ and $u(x,z,t)$, $w(x,z,t)$ are axial and transverse displacements on the neutral plane and arbitrary plane z at cross-section x; θ is rotation of the cross-section; strains and stresses are $\varepsilon_x, \gamma_{xz}, \sigma_x, \tau_{xz}$; the actual position of neutral plane measured from the midplane of beam is denoted by h_0; geometry correction factor is κ.

The homogeneous Timoshenko beam element is used to model the piezoelectric layer

[28], for which the constitutive relations can be formulated as

$$\begin{aligned}
&w_p(x,\bar{z},t)=w_{p0}(x,t);\\
&u_p(x,\bar{z},t)=u_{p0}(x,t)-\theta_p(x,t)\bar{z};\\
&\sigma_{px}=C_{11}^p\varepsilon_{px}-h_{13}D;\\
&\tau_p=\gamma_p C_{55}^p;\\
&\varepsilon_{px}=u'_{p0}-\theta'_p\bar{z},\\
&\gamma_p=w'_{p0}-\theta_p;\\
&\in=-\varepsilon_{px}h_{13}+D\beta_{33}^p,
\end{aligned}\tag{3}$$

where $C_{11}^p, h_{13}, \beta_{33}^p$ denote the elastic, piezoelectric, and dielectric coefficients, respectively, while $\in$ and D represent the electric field and electric displacement within the piezoelectric layer.

Under the assumption of perfect bonding between the host beam and the piezoelectric layer, the continuity conditions can be expressed as

$$\begin{aligned}
&u\left(x,\frac{h_b}{2},t\right)=u_p\left(x,-\frac{h_p}{2},t\right),\\
&w\left(x,\frac{h_b}{2},t\right)=w_p\left(x,-\frac{h_p}{2},t\right)
\end{aligned}\tag{4}$$

that yield $u_{p0}=u_0-\frac{\theta h}{2}$, $h=(h_b+h_p)$,

$$\begin{aligned}
&w_{p0}=w_0,\ \theta=\theta_p\ \text{and}\\
&\varepsilon_{px}=u'_0-\left(\bar{z}+\frac{h}{2}\right)\theta',\ \gamma_p=w'_0-\theta.
\end{aligned}\tag{5}$$

Accordingly, for the coupled beam, the total strain and kinetic energies are given by $\Pi=\Pi_b+\Pi_p$ and $T=T_b+T_p$ that are then put into Hamilton's principle $\int_{t_1}^{t_2}\delta(T+W-\Pi)dt=0$,

where $W=\int_0^L\delta(x-x_0)w_0(x,t)P(t)dx$ is the work done by the concentrated at x_0 force $P(t)$, allowing one to obtain the equations [12]

$$\begin{aligned}
&(I_{11}^*\ddot{u}_0-A_{11}^*u''_0)-(I_{12}^*\ddot{\theta}-A_{12}^*\theta'')=0;\\
&(\ddot{u}_0I_{12}^*-u''_0A_{12}^*)-(\theta\ddot{I}_{22}^*-\theta''A_{22}^*)+(w'_0-\theta)A_{33}^*=0;\\
&\ddot{w}_0I_{11}^*-(w''_0-\theta')A_{33}^*=\delta(x-x_0)P(t),\\
&h_{13}(u'_0+h\theta')-\beta_{33}^pD=0
\end{aligned}\tag{6}$$

with

$$\begin{aligned}
&A_{11}^*=A_bE_b\varphi_{11}(r_e,n)+E_pA_p,\\
&A_{12}^*=\frac{E_pA_ph_p}{2};\\
&E_p=C_{11}^p-\frac{h_{13}^2}{\beta_{33}^p};\\
&A_{22}^*=bh_b^3E_b\varphi_{22}(r_e,n)+C_{11}^pI_p+\frac{E_pA_ph^2}{4};\\
&A_{33}^*=\kappa A_bG_b\varphi_{11}(r_g,n)+C_{55}^pA_p,\\
&I_{11}^*=I_{11}+\rho_pA_p;\\
&I_{12}^*=I_{12}+\frac{\rho_pA_ph}{2};\\
&I_{22}^*=I_{22}+\rho_pI_p+\frac{\rho_pA_ph^2}{4};\\
&I_{11}=\rho_bA_b\varphi_{11}(r_p,n);\\
&I_{12}=\rho_bbh_b^3\varphi_{12}(r_p,n);\\
&I_{22}=\rho_bbh_b^3\varphi_{22}(r_p,n);\\
&\varphi_{11}(x,n)=\frac{x+n}{1+n};\\
&\varphi_{12}(x,n)=\frac{(2x+n)}{2(2+n)}-\frac{\alpha(x+n)}{(1+n)};\\
&\varphi_{22}(x,n)=\frac{3x+n}{3(3+n)}-\frac{\alpha(2x+n)}{(2+n)}+\frac{\alpha^2(x+n)}{(1+n)};\\
&r_p=\frac{\rho_t}{\rho_b};\quad r_e=\frac{E_t}{E_b};\quad r_g=\frac{G_t}{G_b};\\
&\alpha=\frac{1}{2}+\frac{h_0}{h_b};\ h_0=\frac{n(r_e-1)h}{2(n+2)(n+r_e)};\\
&A_b=bh_b;\quad A_p=bh_p;
\end{aligned}\tag{7}$$

Under the Fourier transform, Eq. (6) gets the form

$$\begin{aligned}
&[\mathbf{A}]\{\mathbf{Z}''(x,\omega)\}+[\mathbf{B}]\{\mathbf{Z}'(x,\omega)\}\\
&\qquad+[\mathbf{C}]\{\mathbf{Z}(x,\omega)\}=\{\mathbf{Q}(x,\omega)\}
\end{aligned}\tag{8}$$

where vectors

$$\begin{aligned}
\mathbf{Z}&=\{U(x,\omega),\Theta(x,\omega),W(x,\omega)\}^T\\
&=\int_{-\infty}^{\infty}\{u_0(x,t),\theta(x,t),w_0(x,t)\}e^{-i\omega t}dt,
\end{aligned}$$

$$\mathbf{Z}'=\frac{d\mathbf{z}}{dx},$$

$$\mathbf{Z}''=\frac{d^2\mathbf{z}}{dx^2};$$

$$\{\mathbf{Q}(x,\omega)\} = \delta(x-x_0)\{0,0,\bar{P}(\omega)\}^T$$

and matrices

$$[\mathbf{A}] = \begin{bmatrix} A_{11}^* & -A_{12}^* & 0 \\ -A_{12}^* & A_{22}^* & 0 \\ 0 & 0 & A_{33}^* \end{bmatrix};$$

$$[\mathbf{B}] = \begin{bmatrix} 0 & 0 & 0 \\ 0 & 0 & A_{33}^* \\ 0 & -A_{33}^* & 0 \end{bmatrix};$$

$$[\mathbf{C}] = \begin{bmatrix} \omega^2 I_{11}^* & -\omega^2 I_{12}^* & 0 \\ -\omega^2 I_{12}^* & \omega^2 I_{22}^* - A_{33}^* & 0 \\ 0 & 0 & \omega^2 I_{11}^* \end{bmatrix}.$$

The resulting electric charge can be evaluated when distributed sensing is performed using the piezoelectric layer, as follows

$$Q(\omega) = \int D dA = \int_0^L D dx b = \left(\frac{bh_{13}}{\beta_{33}^p}\right)\left[U(x,\omega) - \frac{h}{2}\Theta(x,\omega)\right]_0^L \quad (9)$$

Consider an FGM beam element containing a crack located at a position *e* from the left end. In recent studies [4, 5], a rotational spring model for the crack has been adopted, with its stiffness determined based on the crack depth. However, due to the inherent coupling between axial and transverse vibrations in FGM beams, the presence of a crack may also influence the axial vibration behavior. Therefore, in the present study, the crack is modeled by a pair of equivalent springs with stiffnesses T and R, corresponding to the translational and rotational components, respectively. Accordingly, the conditions at the crack location can be expressed as [6]

$$\begin{aligned} & W(e+0) = W(e-0), \\ & \Theta(e+0) = \Theta(e-0) + \Theta'_x(e)\gamma_2, \\ & U(e+0) = U(e-0) + U'_x(e)\gamma_1, \\ & W'_x(e+0) = W'_x(e-0) + \Theta'_x(e)\gamma_2, \\ & \Theta'_x(e+0) = \Theta'_x(e-0), \\ & U'_x(e+0) = U'_x(e-0), \\ & \gamma_2 = \frac{A_{22}}{R}, \quad \gamma_1 = \frac{A_{11}}{T}. \end{aligned} \quad (10)$$

Depending on the material parameters, particularly the elastic modulus, the crack compliances γ_1, γ_2 are defined. They coincide with those of a homogeneous beam when $E_t = E_0 = E_b$. By employing Eq. (7), these parameters can be expressed in the following form

$$\begin{aligned} & \gamma_1 = \frac{A_{11}}{T} = \varphi_{11}(r_e,n)\gamma_a, \\ & \gamma_2 = \frac{A_{22}}{R} = \varphi_{22}(r_e,n)\gamma_b, \end{aligned} \quad (11)$$

where $\gamma_a = \frac{E_b A}{T}$ and $\gamma_b = \frac{E_b I_b}{R}$, and the functions φ_{11}, φ_{22} are specified in Eq. (7). The crack magnitudes reduce to the following expressions for a homogeneous beam $(r_e = 1)$

$$\gamma_1 = \gamma_a \varphi_{11}(1,0) = \gamma_a = \gamma_{a0}; \ \gamma_2 = \gamma_b \varphi_{22}(1,0) = \frac{\gamma_b}{12} = \gamma_{b0},$$

which are expressed in terms of the crack depth (a) for flexural [24] and axial [20] vibration cases as follows

$$\begin{aligned} & \gamma_{a0} = \frac{AE_0}{T} = f_1(z) 2\pi h_b (1-\nu_0^2), \\ & \gamma_{b0} = \frac{I_0 E_0}{R} = f_2(z) 6\pi h_b (1-\nu_0^2), \\ & z = \frac{a}{h_b}, \\ & f_1(z) = z^2 \begin{pmatrix} 92.3552z^8 - 146.682z^7 \\ +139.123z^6 - 67.47z^5 \\ +31.5685z^4 - 10.7054z^3 \\ +5.92134z^2 - 0.17248z + 0.6272 \end{pmatrix}; \\ & f_2(z) = z^2 \begin{pmatrix} 19.6z^8 - 40.7556z^7 \\ +47.1063z^6 - 33.0351z^5 \\ +20.2948z^4 - 9.9736z^3 \\ +4.5948z^2 - 1.04533z + 0.6272 \end{pmatrix}; \\ & \gamma_1 = \gamma_{a0}\left(\frac{a}{h_b}\right)\varphi_{11}(r_e,n); \\ & \gamma_2 = 12\gamma_{b0}\left(\frac{a}{h_b}\right)\varphi_{22}(r_e,n). \end{aligned} \quad (12)$$

Accordingly, the crack magnitudes are formulated in the vibration analysis of cracked

FGM beams, as

$$\gamma_1 = \gamma_{a0}\left(\frac{a}{h_b}\right)\varphi_{11}(r_e,n);$$
$$\gamma_2 = 12\gamma_{b0}\left(\frac{a}{h_b}\right)\varphi_{22}(r_e,n). \quad (13)$$

The crack magnitudes γ_1,γ_2 calculated in Eq. (13) depend on both the material properties and geometric characteristics of the FGM beam. When $r_e = 1$ or $E_t = E_b = E_0$, these parameters reduce to those of a homogeneous beam.

3. General solution for vibration shape of cracked FGM beam with piezoelectric layer

Seeking solutions of homogeneous Eq. (8) in the form: $\mathbf{Z}_0 = \mathbf{d}e^{\lambda x}$ leads to characteristic equation [8]

$$\det\left[\lambda^2\mathbf{A} + \lambda\mathbf{B} + \mathbf{C}\right] = 0. \quad (14)$$

This equation represents a cub algebraic equation in terms of $\eta = \lambda^2$ which can be readily solved to obtain three roots η_1,η_2,η_3. Accordingly, one obtains $\lambda_{1,4} = \pm k_1; \lambda_{2,5} = \pm k_2; \lambda_{3,6} = \pm k_3$; $k_j = \sqrt{\eta_j}, j = 1,2,3$. Hence, the general solution of Eq. (8) can be expressed as

$$\{\mathbf{Z}_0\} = \begin{bmatrix} d_{11} & d_{12} & \cdots & d_{16} \\ d_{21} & d_{22} & \cdots & d_{26} \\ d_{31} & d_{32} & \cdots & d_{36} \end{bmatrix}\begin{Bmatrix} e^{\lambda_1 x} \\ \vdots \\ e^{\lambda_6 x} \end{Bmatrix}$$
$$= \begin{bmatrix} \alpha_1 C_1 & \alpha_2 C_2 & \cdots & \alpha_6 C_6 \\ C_1 & C_2 & \cdots & C_6 \\ \beta_1 C_1 & \beta_2 C_2 & \cdots & \beta_6 C_6 \end{bmatrix}\begin{Bmatrix} e^{\lambda_1 x} \\ \vdots \\ e^{\lambda_6 x} \end{Bmatrix}$$

with constants $C_1,\dots,C_6$ and

$$\alpha_j = \frac{\omega^2 I_{11}^* + \lambda_j^2 A_{11}^*}{\omega^2 I_{12}^* + \eta_j A_{12}^*};\ \beta_j = \frac{\lambda_j A_{33}^*}{\omega^2 I_{11}^* + \lambda_j^2 A_{33}^*};\ j = 1,2,3.$$

The latter expressions show that

$$\alpha_4 = \alpha_1; \alpha_5 = \alpha_2; \alpha_6 = \alpha_3; \beta_4 = -\beta_1; \beta_5 = -\beta_2; \beta_6 = -\beta_3.$$

Therefore, general solution of (8) can be rewritten in the form

$$\{\mathbf{Z}_0(x,\omega)\} = [\mathbf{G}_0(x,\omega)]\{\mathbf{C}\} \quad (15)$$

where

$$[G_0(x,\omega)] = \begin{bmatrix} \alpha_1 e^{k_1 x} & \alpha_2 e^{k_2 x} & \alpha_3 e^{k_3 x} & \alpha_1 e^{-k_1 x} & \alpha_2 e^{-k_2 x} & \alpha_3 e^{-k_3 x} \\ e^{k_1 x} & e^{k_2 x} & e^{k_3 x} & e^{-k_1 x} & e^{-k_2 x} & e^{-k_3 x} \\ \beta_1 e^{k_1 x} & \beta_2 e^{k_2 x} & \beta_3 e^{k_3 x} & -\beta_1 e^{-k_1 x} & -\beta_2 e^{-k_2 x} & -\beta_3 e^{-k_3 x} \end{bmatrix} \quad (16)$$

and $\{\mathbf{C}\} = (C_1,\dots,C_6)^T$.

In Eq. (8), a particular solution $Z_c(x,\omega)$ is sought such that it satisfies the following conditions

$$\{\mathbf{Z}_c(0)\} = \left(\gamma_a U_0'(e), \gamma_b\theta_0'(e), 0\right)^T; \quad (17)$$
$$\{\mathbf{Z}_c'(0)\} = \left(0, 0, \gamma_b\theta_0'(e)\right)^T.$$

By substituting Eq. (15) into Eq. (17), one obtains

$$\{\mathbf{Z}_c(x,\omega)\} = [\mathbf{G}_c(x,\omega)]\{\mathbf{Z}_0'(e,\omega)\} \quad (18)$$

where

$$[\mathbf{G}_c(x,\omega)] = \begin{bmatrix} \gamma_a\sum_{i=1}^{3}\alpha_i\delta_{i1}\cosh(k_i x) & \gamma_b\sum_{i=1}^{3}\alpha_i(\delta_{i2}+\delta_{i3})\cosh(k_i x) & 0 \\ \gamma_a\sum_{i=1}^{3}\delta_{i1}\cosh(k_i x) & \gamma_b\sum_{i=1}^{3}(\delta_{i2}+\delta_{i3})\cosh(k_i x) & 0 \\ \gamma_a\sum_{i=1}^{3}\beta_i\delta_{i1}\sinh(k_i x) & \gamma_b\sum_{i=1}^{3}\beta_i(\delta_{i2}+\delta_{i3})\sinh(k_2 x) & 0 \end{bmatrix} \quad (19)$$

and

$$\delta_{11} = \frac{k_3\beta_3 - k_2\beta_2}{\Delta};\ \delta_{12} = \frac{\alpha_3 k_2\beta_2 - \alpha_2 k_3\beta_3}{\Delta};$$
$$\delta_{13} = \frac{\alpha_2 - \alpha_3}{\Delta};\ \delta_{21} = \frac{k_1\beta_1 - k_3\beta_3}{\Delta};$$
$$\delta_{22} = \frac{\alpha_1 k_3\beta_3 - \alpha_3 k_1\beta_1}{\Delta};\ \delta_{23} = \frac{\alpha_3 - \alpha_1}{\Delta};$$
$$\delta_{31} = \frac{k_2\beta_2 - k_1\beta_1}{\Delta};\ \delta_{32} = \frac{\alpha_2 k_1\beta_1 - \alpha_1 k_2\beta_2}{\Delta};$$

$$\delta_{33} = \frac{\alpha_1 - \alpha_2}{\Delta};$$

$$\Delta = k_1\beta_1(\alpha_2 - \alpha_3) + k_2\beta_2(\alpha_3 - \alpha_1) + k_3\beta_3(\alpha_1 - \alpha_2).$$

Accordingly, it can be verified that the solution of Eq. (8), satisfying the conditions in Eq. (10), is given by

$$\{\mathbf{Z}(x,\omega)\} = \begin{cases} \{\mathbf{Z}_0(x,\omega)\} + \{\mathbf{Z}_c(x-e,\omega)\}: & \text{for } e \le x \\ \{\mathbf{Z}_0(x,\omega)\}: & \text{for } e > x \end{cases}$$

that can be rewritten in the form

$$\begin{aligned}\{\mathbf{Z}(x,\omega)\} &= [\mathbf{K}(x-e)]\cdot\{\mathbf{Z}_0'(e,\omega)\} + \{\mathbf{Z}_0(x,\omega)\} \\ &= [\mathbf{\Phi}(x,\omega)]\{\mathbf{C}\},\end{aligned} \tag{20}$$

with the matrices introduced

$$[\mathbf{\Phi}(x,\omega)] = \left[\mathbf{K}(x-e)]\mathbf{G}_0'(x,\omega) + \mathbf{G}_0(x,\omega)\right];$$

$$[\mathbf{K}(x)] = \begin{cases}[\mathbf{0}]: & 0 \ge x; \\ [\mathbf{G}_c(x)]: & 0 < x;\end{cases} \tag{21}$$

$$[\mathbf{K}'(x)] = \begin{cases}[\mathbf{0}]: & 0 \ge x; \\ [\mathbf{G}_c'(x)]: & 0 < x.\end{cases}$$

By following a similar procedure, the general solution for the free vibration of a beam containing multiple cracks can be obtained in the form of Eq. (20), as

$$\begin{aligned}\left[\mathbf{M}_j\right] &= \sum_{k=1}^{j-1}\left[\mathbf{G}_c'\left(e_j - e_k\right)\right][\mathbf{M}_k] + \left[\mathbf{G}_0'\left(e_j,\omega\right)\right], \\ \left[\mathbf{\Phi}(x,\omega)\right] &= \sum_{j=1}^{n}\left[\mathbf{K}\left(x - e_j\right)\right]\left[\mathbf{M}_j\right] + \left[\mathbf{G}_0(x,\omega)\right].\end{aligned} \tag{22}$$

4. EMR of cracked piezoelectric functionally graded beams

Furthermore, it is well known that general solution of inhomogeneous Eq. (8) can be found in the form

$$\{\mathbf{Z}_P(x,\omega)\} = [\mathbf{\Phi}(x,\omega)]\{\mathbf{C}\} + \{\mathbf{Z}_q(x,\omega)\} \tag{23}$$

with a particular solution

$$\mathbf{Z}_q(x,\omega) = \{U_q(x,\omega), \Theta_q(x,\omega), W_q(x,\omega)\}^T$$

and by given boundary conditions, the constant vector $\{\mathbf{C}\} = \{C_1,\dots,C_6\}^T$ is obtained.

In case of concentrated load

$$\{\mathbf{Q}(x,\omega)\} = \{\bar{\mathbf{Q}}(\omega)\}\delta(x - x_0)$$

with $\{\bar{\mathbf{Q}}(\omega)\} = \{0,0,\bar{P}(\omega)\}^T$, the particular solution $\mathbf{Z}_q(x,\omega)$ is obtained by

$$\{\mathbf{Z}_q(x,\omega)\} = \bar{P}(\omega)\{\mathbf{h}_3(x - x_0,\omega)\}, \tag{24}$$

where vector function $\mathbf{h}_3(x,\omega)$ is solutions of homogeneous Eq. (8) satisfying conditions

$$\{h_3(0,\omega)\} = \{0\};$$

$$[A]\{h_3'(0,\omega)\} = \{0,0,1\}^T.$$

Namely, it can be found as

$$\{\mathbf{h}_3(x,\omega)\} = [\mathbf{H}_3(x,\omega)]\{\mathbf{d}\}, \tag{25}$$

$$[\mathbf{H}_3(x,\omega)] = \begin{bmatrix}\phi_{11}+\phi_{14} & \phi_{12}+\phi_{15} & \phi_{13}+\phi_{16} \\ \phi_{21}+\phi_{24} & \phi_{22}+\phi_{25} & \phi_{23}+\phi_{26} \\ \phi_{31}+\phi_{34} & \phi_{32}+\phi_{35} & \phi_{33}+\phi_{36}\end{bmatrix};$$

$$\{\mathbf{d}\} = \frac{1}{2\Delta}\begin{Bmatrix}\alpha_2 - \alpha_3 \\ \alpha_3 - \alpha_1 \\ \alpha_1 - \alpha_2\end{Bmatrix} \tag{26}$$

with $\phi_{ij}, i,j = 1,\dots,6$ are elements of matrix $\left[\mathbf{\Phi}(x,\omega)\right]$ defined by Eq. (21) and

$$\Delta = A_{33}^*\begin{bmatrix}\beta_1k_1(\alpha_2-\alpha_3) + \beta_2k_2(\alpha_3-\alpha_1) \\ +\beta_3k_3(\alpha_1-\alpha_2)\end{bmatrix}.$$

Hence, general solution (23) can be rewritten as

$$\begin{aligned}\{\mathbf{Z}_P(x,x_0,\omega)\} &= [\mathbf{\Phi}(x,\omega)]\{\mathbf{C}\} \\ &+ \bar{P}(\omega)[\mathbf{H}_3(x - x_0,\omega)]\{\mathbf{d}\}.\end{aligned} \tag{27}$$

By applying the boundary conditions expressed through the operator $\mathcal{B}\left\{\mathbf{Z}_p(x,\omega)\right\} = 0$ to the solution in Eq. (27), the constant vector $\{\mathbf{C}\}$ can be determined as

$$\{\mathbf{C}\} = -\bar{P}(\omega)\left[\mathbf{B\Phi}(\omega)\right]^{-1}\left[\mathbf{BH}(x_0,\omega)\right]\{\mathbf{d}\}, \tag{28}$$

where

$$\left[\mathbf{B\Phi}(\omega)\right] = \mathcal{B}\left[\mathbf{\Phi}(x,\omega)\right],$$

$$\left[\mathbf{BH}(x_0,\omega)\right] = \mathcal{B}\left[\mathbf{H}_3(x - x_0,\omega)\right].$$

The latter matrices are provided for different boundary conditions. Thus, solution (27) with constant vector (28) gets the form

$$\{\mathbf{Z}_p(x,x_0,\omega)\} = \bar{P}(\omega)\left[\mathbf{\Psi}(x,x_0,\omega)\right]\{\mathbf{d}\}, \tag{29}$$

where

$$\left[\mathbf{\Psi}(x,x_0,\omega)\right]=\left[\mathbf{H}_3(x-x_0,\omega)\right] \\ -\left[\mathbf{\Phi}(x,\omega)\right]\left[\mathbf{B\Phi}(\omega)\right]^{-1}\left[\mathbf{BH}(x_0,\omega)\right]. \quad (30)$$

As is well known, the conventional frequency response function vector is defined by

$$\mathbf{FRF}(x,x_0,\omega)=\{\mathbf{Z}_p(x,x_0,\omega)\}/\bar{P}(\omega) \\ =\left[\mathbf{\Psi}(x,x_0,\omega)\right]\{\mathbf{d}\} \\ =\left\{U_p(x,x_0,\omega),\Theta_p(x,x_0,\omega),W_p(x,x_0,\omega)\right\}^T, \quad (31)$$

that has three components: $U_p(x,x_0,\omega)$ - longitudinal, $\Theta_p(x,x_0,\omega)$ - slope and $W_p(x,x_0,\omega)$ - deflection frequency response functions (FRFs). Based on the mechanical frequency response functions, the electric charge generated in the piezoelectric layer, referred to as EMR, can be evaluated as

$$\mathrm{EMR}(x_0,\omega)=Q(x_0,\omega) \\ =\left(\frac{bh_{13}}{\beta_{33}^p}\right)\int_0^L\left[U_p'(x,x_0,\omega)+h\Theta_p'(x,x_0,\omega)\right]dx \\ =\frac{bh_{13}}{\beta_{33}^p}\left\{\begin{bmatrix}U_p(L,x_0,\omega)-\Theta_p(0,x_0,\omega)\\ -\gamma_1(a)U_p'(e,x_0,\omega)\end{bmatrix} \\ +h\begin{bmatrix}\Theta_p(L,x_0,\omega)-\Theta_p(0,x_0,\omega)\\ -\gamma_2(a)\Theta_p'(e,x_0,\omega)\end{bmatrix}\right\} \quad (32)$$

In case of multiple cracked piezoelectric FGM beams, the EMR is

$$\mathrm{EMR}(x_0,\omega)=\frac{bh_{13}}{\beta_{33}^p}\left\{\begin{array}{l}U_p(L,x_0,\omega)-U_p(0,x_0,\omega)\\ +h\left[\Theta_p(L,x_0,\omega)-\Theta_p(0,x_0,\omega)\right]\\ -\sum_{j=1}^{m}\begin{bmatrix}\gamma_1(a_j)U_p'(e_j,x_0,\omega)\\ +\gamma_2(a_j)\Theta_p'(e_j,x_0,\omega)\end{bmatrix}\end{array}\right\} \quad (33)$$

with crack magnitudes γ_1, γ_2 defined above in Eq. (12) - (13). The latter Eq. (32) can be rewritten in the form

$$F_Q(x_0,e,a,\omega)=F_Q^0(x_0,\omega) \\ -\gamma_1(a)Q_u'(e,x_0,\omega)-\gamma_2(a)Q_\theta'(e,x_0,\omega), \quad (34)$$

where

$$Q_u'(e,x_0,\omega)=\left(\frac{bh_{13}}{\beta_{33}^p}\right)U_p'(e,x_0,\omega);$$

$$Q_\theta'(e,x_0,\omega)=\left(\frac{bh_{13}}{\beta_{33}^p}\right)h\Theta_p'(e,x_0,\omega)$$

and

$$F_Q^0(x_0,\omega)=\left(\frac{bh_{13}}{\beta_{33}^p}\right)\begin{bmatrix}U_p(L,x_0,\omega)-U_p(0,x_0,\omega)\\ +h\Theta_p(L,x_0,\omega)\\ -h\Theta_p(0,x_0,\omega)\end{bmatrix} \quad (35)$$

It is evident that the functions $F_Q^0(x_0,\omega)$ and $F_Q(x_0,e,a,\omega)$ defined in Eqs. (34)–(35), correspond to the EMR of intact and cracked beams, respectively, and both depend on the loading position x_0. This property enables a more efficient evaluation of mechanical receptance, as it avoids the necessity of measuring structural responses at predefined positions. In addition, Eq. (34) indicates that the EMR of a damaged beam is directly related to crack characteristics, including its position and size, which makes it a practical indicator for identifying structural damage through electro-mechanical response analysis.

5. Numerical results and discussion

Consider an FGM beam bonded with a piezoelectric layer, as illustrated in Fig. 1. Recalling the notation for the thicknesses of the piezoelectric layer and the host beam, it can be observed that a single beam without a piezoelectric layer represents a special case of the two-layer system when $h_p = 0$. Accordingly, the FGM beam with a piezoelectric layer is treated as a two-layer beam with the following properties

$E_t = 390\text{MPa}, \rho_t = 3960\text{kg/m}^3, \mu_t = 0.25;$
$E_b = 210\text{MPa}, \rho_b = 7800\text{kg/m}^3, \mu_b = 0.31;$
$C_{55}^p = 21.0526\text{GPa}, C_{11}^p = 69.0084\text{GPa},$
$h_{13} = -7.70394\times10^8\,\text{V/m}, \rho_p = 7750\text{kg/m}^3,$

Numerical analysis completed below addresses two questions: first is to consider the correlation between electrical charge induced in the piezoelectric layer and mechanical deflection of the beam under a concentrated unit force along the load applying point, material grading index and crack parameters. The second one is to examine sensitivity of the EMR to crack in dependence on the material gradient index and loading position. First, spectrums of the midspan mechanical deflection and electrical charge produced in the piezoelectric layer under concentrated load are examined for the cracked FGM beam in dependence upon location of applied load, material gradient index and crack parameters.

5.1. Mechanical and electrical frequency response functions

(a)

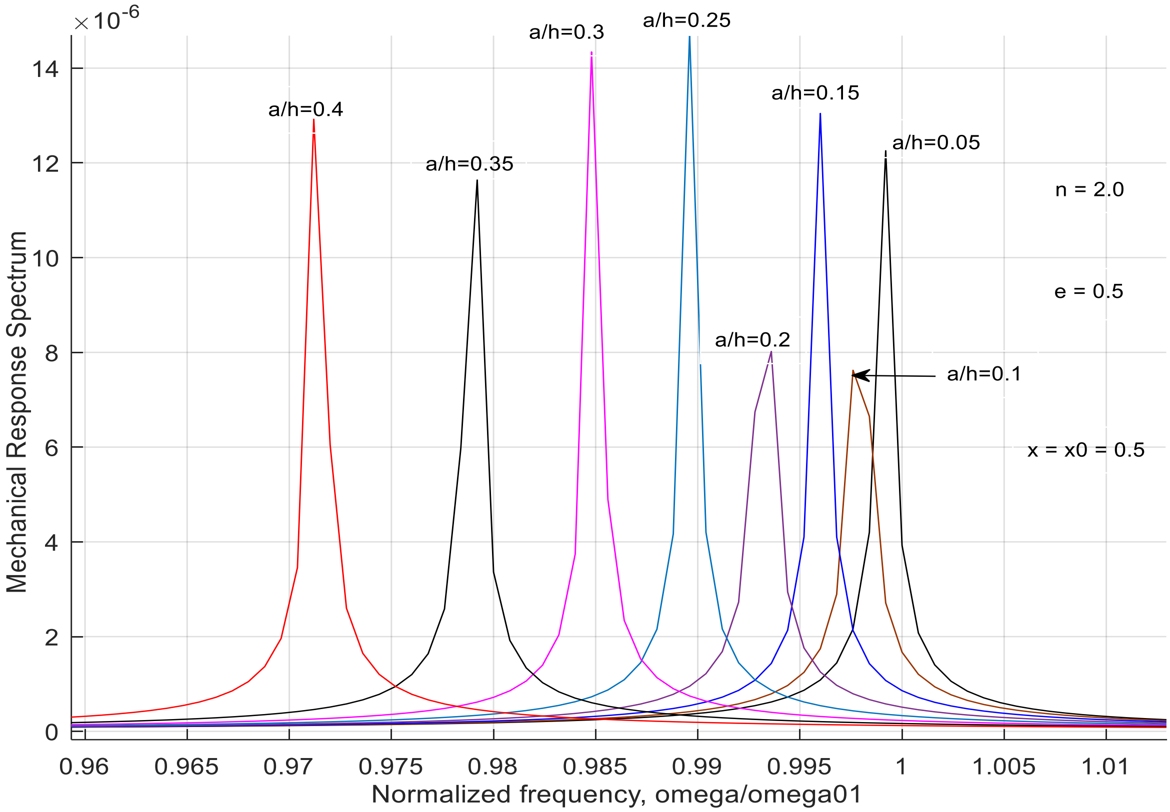

Fig. 2. Spectrums of mechanical midspan deflection (a) and electrical charge response (b) in various crack depth (a/h) for the case of crack position e/L= 0.5, material gradation index n = 2.0 and load applied at midspan ($x_0 = 0.5$).

Spectrums of the mechanical $W_p(L/2, x_0, \omega)$ and electrical $Q(x_0, \omega)$ frequency response functions defined by Eq. (31) and (32) are computed for various crack parameters, material gradient index and position of load application. The frequency dependent functions are examined in the frequency range surrounding the fundamental frequency ω_{01} of the intact beam and illustrated in Figs. 2-4. Graphs presented in the Figures show that all the spectrums attain their local peaks (maximum) at the resonant frequency, whose shift from the undamaged one is dependent on crack and material parameters. Namely, it can be observed from Fig. 2 that resonant frequency is reduced due to crack and its deviation from the fundamental frequency increases with crack depth. Greatest shift of the resonant frequency is reached when crack occurred at the beam center (L/2), see Fig. 3. However, variation of the resonance peak high is non monotonous along the material gradient index, the peak gets to be highest for n = 2 (Fig. 4) compared to that computed for other values of material gradient index. Numerical analysis demonstrates also the fact that the spectrums have unimportant modification due to position of load application. This is because external excitation does not modify the spectral structure of structure's response. Finally, it can be seen a similarity in spectral structure of the mechanical and electrical responses which would be examined in subsequent subsection.

(b)

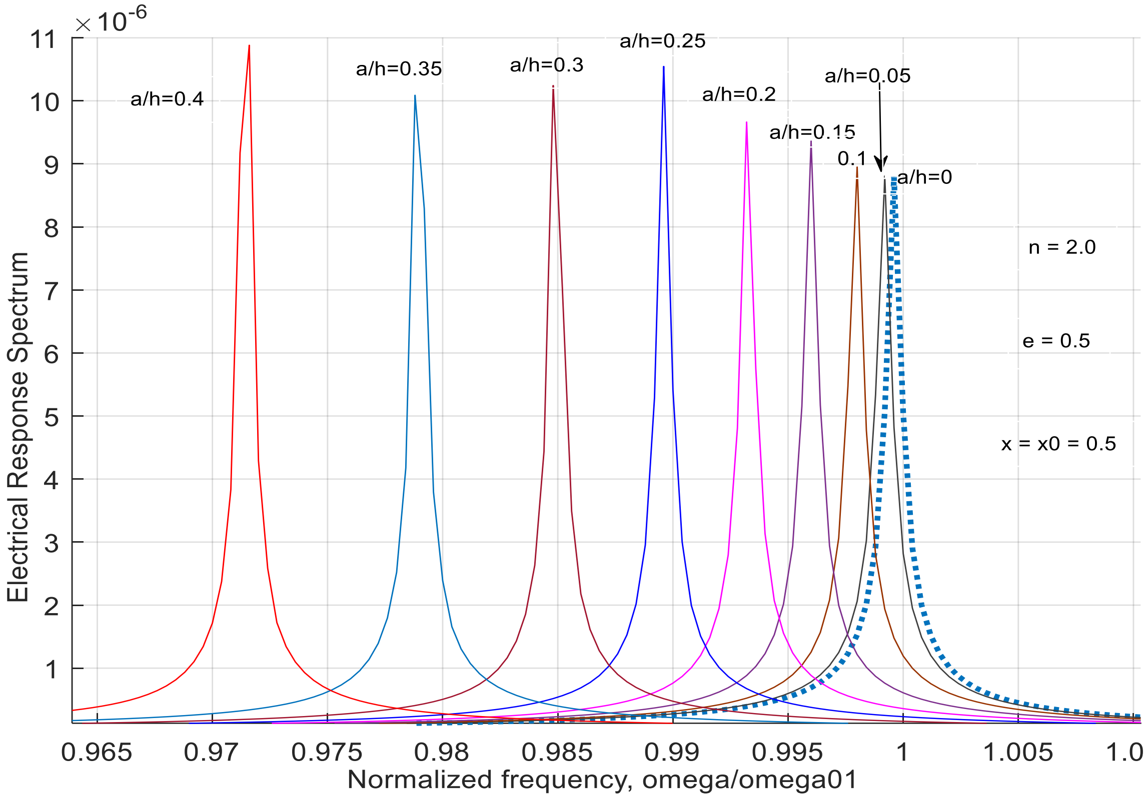

Fig. 2. (continued)

(a)

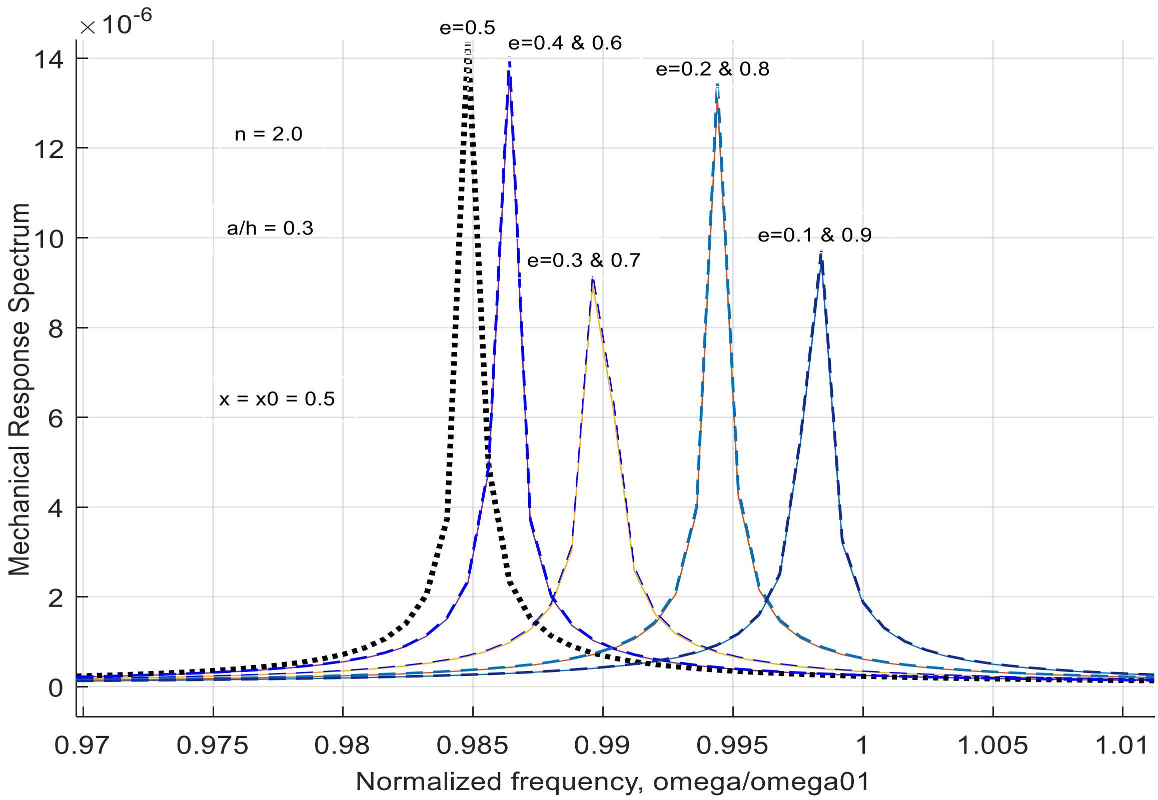

Fig. 3. Spectrums of mechanical midspan deflection (a) and electrical charge response (b) in various crack location (e/L) for the case of crack depth a/h = 0.3, material gradation index n = 2.0 and load applied at midspan ($x_0 = 0.5$).

(b)

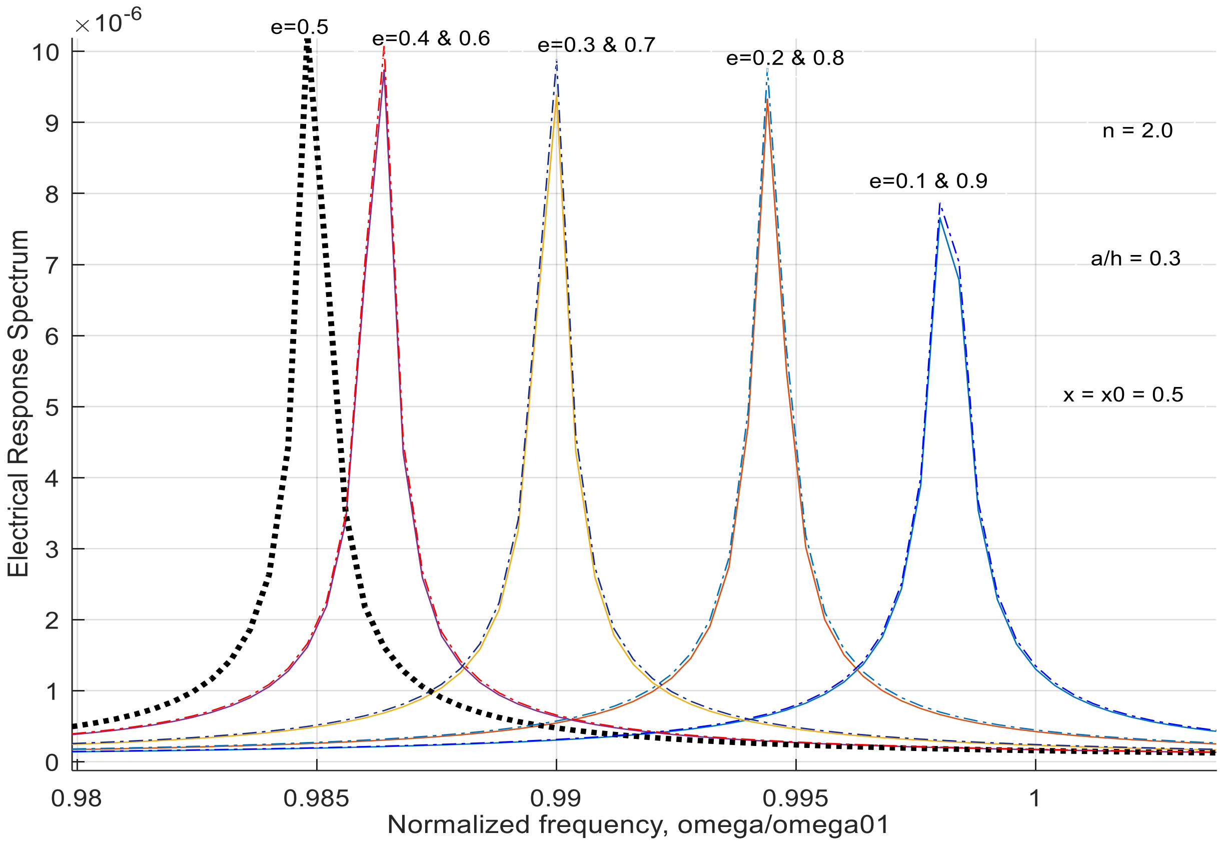

Fig. 3. (continued)

(a)

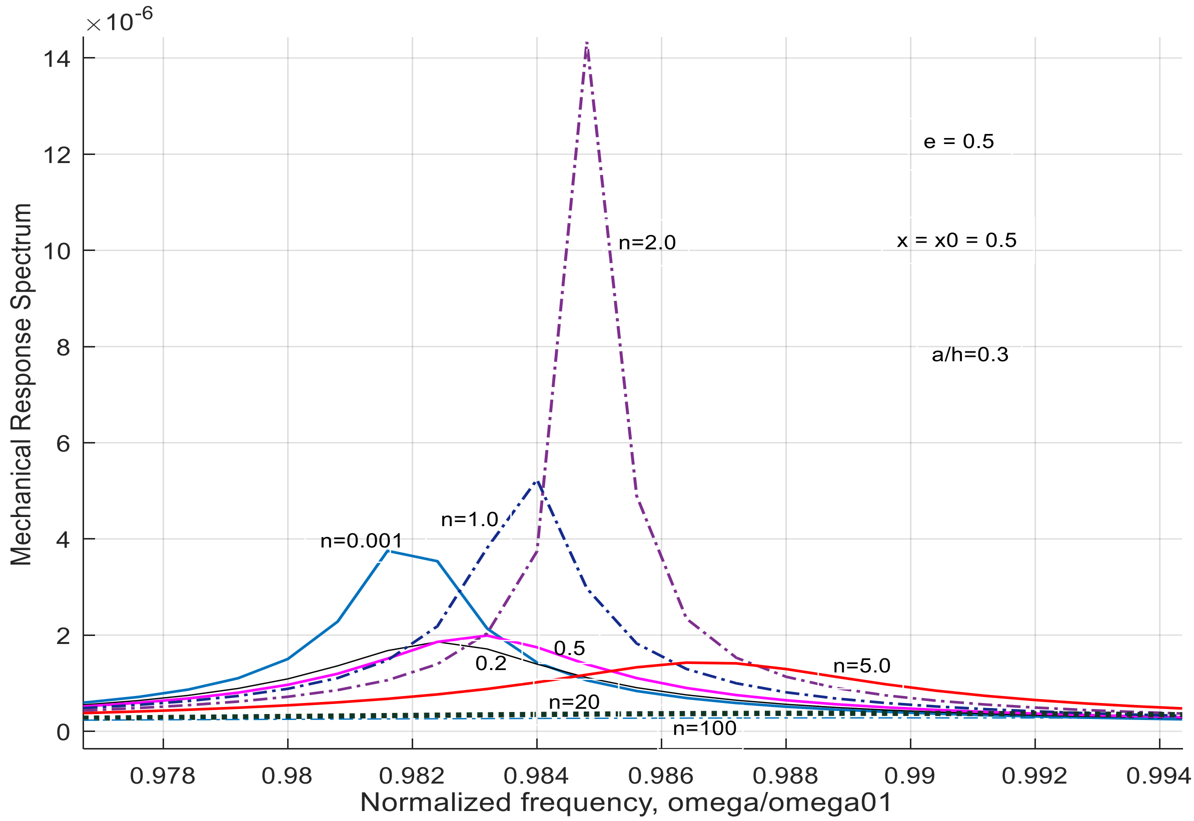

Fig. 4. Spectrums of mechanical midspan deflection (a) and electrical charge response (b) in various material gradation index (n) in the case of crack depth a/h = 0.3, crack location (e/L= 0.5) and load applied at midspan (x_0=0.5).

(b)

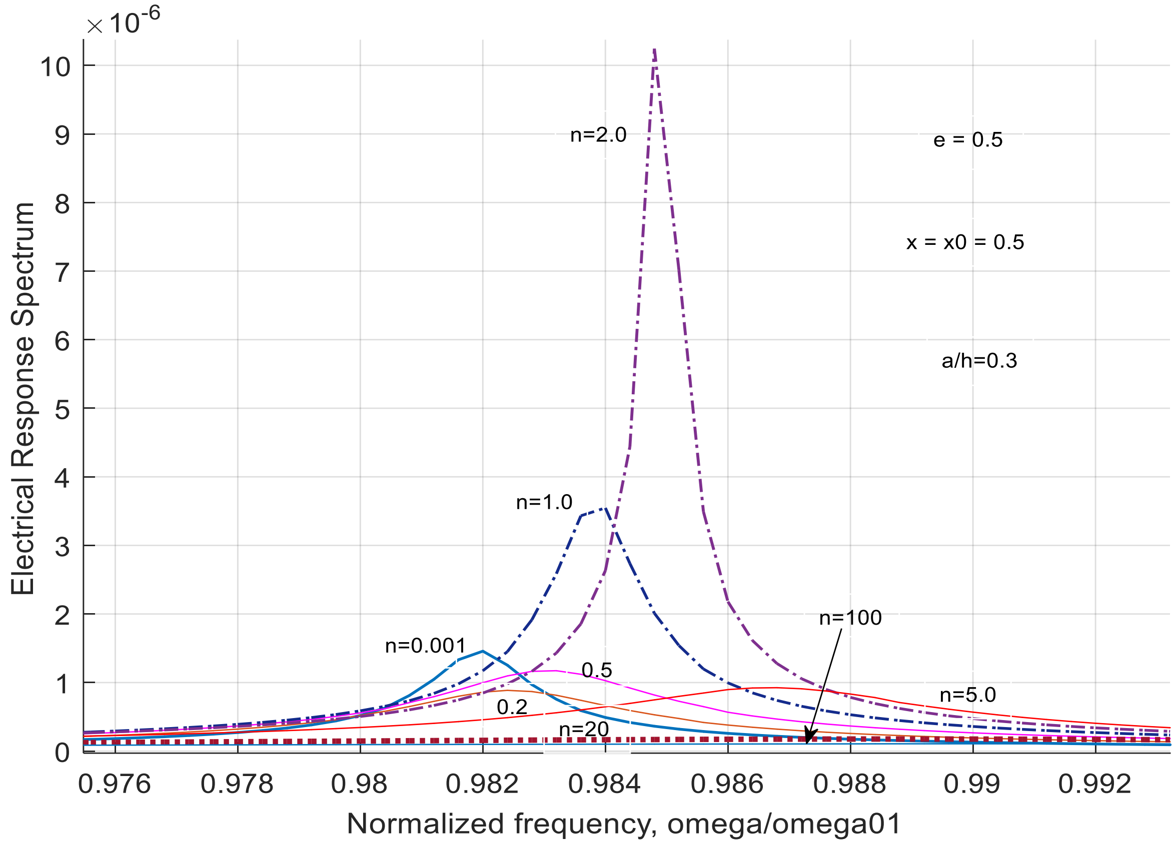

Fig. 4. (continued)

5.2. Spectral similarity of mechanical and electrical frequency responses

Similarity of two signals $X=\{X_1,...,X_N\}$, $Y=\{Y_1,...,Y_N\}$ can be characterized by coefficient

$$\lambda_{XY}=\left[\left(\sum_{k=1}^{N}X_kY_k\right)^2\Big/\left(\sum_{k=1}^{N}X_k^2\sum_{k=1}^{N}Y_k^2\right)\right]^{1/2} \quad (36)$$

It is easy to verify that $0<\lambda_{XY}\le 1$ and $\lambda_{XY}=1$ only if $X=\alpha Y$. Two signals are regarded as similar if $\lambda_{XY}\approx 1$ and its deviation from unit denotes the dissimilarity degree of the signals. Two frequency dependent signals $W(\omega),Q(\omega)$ can be compared to similarity by using so-called coherence coefficient

$$C_{WQ}=\left[\frac{\left(\sum_{k=1}^{N}W(\omega_k)Q(\omega_k)\right)^2}{\sum_{k=1}^{N}W^2(\omega_k)\sum_{k=1}^{N}Q^2(\omega_k)}\right]^{1/2} \quad (37)$$

The coherence coefficient calculated with mechanical midspan deflection W_p (L/2, x_0, ω) and electric response Q (x_0, ω) given by Eq. (31) and Eq. (32) gives rise a quantity called hereby spectral similarity index of the responses. The spectral similarity index denoted by S_{WQ} (x_0, n, e, a) is a function of the exciting position x_0, material gradient index n and crack parameters such as its location e and depth a.

The similarity index computed for various parameters mentioned above are given in Tables 1-4 which show that the index is very close to unit (almost greater than 0.99 except some cases when the exciting force is applied at the location x_0 = 0.1. The closeness of the spectral similarity index to 1 exhibits a strong similarity of mechanical and electrical response in their spectral structures. This ensures high reliability of using piezoelectric layer as a distributed sensor for measuring mechanical behavior of a structure under consideration.

5.3. Sensitivity of EMR to crack

The coherence coefficient (37) calculated for

EMR $F_Q(x_0, e, a, \omega)$ and $F_Q^0(x_0, \omega) = F_Q(x_0, e, 0, \omega)$ given by Eqs. (34) and (35) respectively for cracked and uncracked beams, gives the coefficient

$$S_Q(e, a), = \left[\frac{\left(\sum_{k=1}^{N} F_Q(\omega_k) F_Q^0(\omega_k) \right)^2}{\sum_{k=1}^{N} F_Q^2(\omega_k) \sum_{k=1}^{N} F_Q^{02}(\omega_k)} \right]^{1/2} \quad (38)$$

that is a function of crack parameters and called therefore sensitivity of EMR to crack. The sensitivity is dependent not only on the crack parameters but also on the applied load position x_0 and material gradient index n.

The EMR sensitivity to crack can be acknowledged as a spectral damage index that will be demonstrated in Figs. 5-6. Graphs depicted in the Figures show that the spectral damage index is robustly sensitive to crack depth (Fig. 5a), it can reduce the damage index to more than 90% by relative crack depth of greater than 30% and only 10% crack depth can decrease the index to 50%. The spectral damage index is most sensitive to crack appeared at the beam's middle (e/L = 0.5) and when material gradient index n = 2.0 (Fig. 5b). For the material gradation index more than 10 the change in the damage index decreases to less than 10%. Position of load application makes no effect on sensitivity of the spectral damage index to crack as shown in Fig. 6.

Table 1. Spectral similarity index of electrical frequency response and mechanical midspan deflection for cracked beam with various loading positions (0.1 – 0.9) and crack depths (0.0 – 0.4).

Exciting posit. x_0	Crack depth (Crack location n = 2.0, e/L= 0.5)								
	0.0	0.05	0.10	0.15	0.20	0.25	0.30	0.35	0.40
0.1	0.9942	0.9942	0.9943	0.9944	0.9946	0.9948	0.9951	0.9955	0.9960
0.2	0.9991	0.9991	0.9991	0.9991	0.9992	0.9992	0.9992	0.9993	0.9993
0.3	0.9997	0.9997	0.9997	0.9997	0.9997	0.9997	0.9997	0.9997	0.9997
0.4	0.9999	0.9999	0.9999	0.9999	0.9999	0.9999	0.9999	0.9999	0.9998
0.5	1.0000	1.0000	1.0000	1.0000	1.0000	0.9999	0.9999	0.9999	0.9999
0.6	1.0000	1.0000	1.0000	1.0000	1.0000	1.0000	0.9999	0.9999	0.9999
0.7	1.0000	1.0000	1.0000	1.0000	1.0000	1.0000	0.9999	0.9999	0.9999
0.8	1.0000	1.0000	1.0000	1.0000	1.0000	1.0000	1.0000	0.9999	0.9999
0.9	1.0000	1.0000	1.0000	1.0000	1.0000	1.0000	1.0000	0.9999	0.9999

Table 2. Spectral similarity index of electrical frequency response and mechanical midspan deflection for cracked beam with various exciting points (0.1 – 0.9) and crack locations (0.1 – 0.9).

Exciting posit. x_0	Crack location (Crack depth a/h= 0.3; n = 2.0.)								
	0.1	0.2	0.3	0.4	0.5	0.6	0.7	0.8	0.9
0.1	0.9941	0.9942	0.9945	0.9949	0.9951	0.9952	0.9953	0.9953	0.9958
0.2	0.9991	0.9991	0.9991	0.9992	0.9992	0.9993	0.9993	0.9993	0.9991
0.3	0.9997	0.9997	0.9997	0.9997	0.9997	0.9997	0.9998	0.9997	0.9997
0.4	0.9999	0.9999	0.9999	0.9999	0.9999	0.9999	0.9999	0.9999	0.9999
0.5	1.0000	0.9999	0.9999	0.9999	0.9999	0.9999	0.9999	1.0000	1.0000
0.6	1.0000	1.0000	1.0000	0.9999	0.9999	0.9999	1.0000	1.0000	1.0000
0.7	1.0000	1.0000	1.0000	1.0000	0.9999	1.0000	1.0000	1.0000	1.0000
0.8	1.0000	1.0000	1.0000	1.0000	1.0000	1.0000	1.0000	1.0000	1.0000
0.9	1.0000	1.0000	1.0000	1.0000	1.0000	1.0000	1.0000	1.0000	1.0000

Table 3. Spectral similarity index of electrical frequency response and mechanical midspan deflection for cracked beam with various exciting points (0.1 – 0.9) and material distribution index (n).

Exciting posit. x0	Material distribution index (n) (Crack depth a/h= 0.3; Crack location e/ L= 0.5)								
	0.001	0.20	0.50	1.0	2.0	5.0	10.0	20.0	100
0.1	0.9829	0.9637	0.9653	0.9860	0.9951	0.9493	0.9001	0.8850	0.8843
0.2	0.9974	0.9942	0.9944	0.9978	0.9992	0.9912	0.9776	0.9681	0.9588
0.3	0.9991	0.9980	0.9981	0.9993	0.9997	0.9970	0.9920	0.9879	0.9829
0.4	0.9996	0.9993	0.9993	0.9997	0.9999	0.9990	0.9973	0.9957	0.9938
0.5	0.9998	0.9997	0.9997	0.9998	0.9999	0.9996	0.9990	0.9984	0.9976
0.6	0.9999	0.9998	0.9998	0.9999	0.9999	0.9998	0.9995	0.9993	0.9989
0.7	0.9999	0.9999	0.9999	0.9999	0.9999	0.9999	0.9997	0.9996	0.9995
0.8	0.9999	0.9999	0.9999	0.9999	1.0000	0.9999	0.9998	0.9998	0.9997
0.9	0.9999	0.9999	0.9999	0.9999	1.0000	0.9999	0.9999	0.9998	0.9998

Table 4. Spectral similarity index of electrical frequency response and mechanical midspan deflection for cracked beam with various material distribution index (n) and crack locations (0.1 – 0.9).
Crack depth a/h = 0.3; exciting point x_0 = 0.5.

Material index, n	Crack location (Crack depth a/h= 0.3; exciting point x_0 = 0.5)								
	0.1	0.2	0.3	0.4	0.5	0.6	0.7	0.8	0.9
0.001	0.9999	0.9999	0.9998	0.9998	0.9998	0.9998	0.9999	0.9999	0.9999
0.2	0.9998	0.9997	0.9997	0.9997	0.9997	0.9997	0.9997	0.9998	0.9998
0.5	0.9998	0.9997	0.9997	0.9997	0.9997	0.9997	0.9997	0.9998	0.9998
1.0	0.9999	0.9999	0.9999	0.9998	0.9998	0.9999	0.9999	0.9999	0.9999
2.0	1.0000	0.9999	0.9999	0.9999	0.9999	0.9999	0.9999	1.0000	1.0000
5.0	0.9996	0.9996	0.9996	0.9996	0.9996	0.9996	0.9996	0.9996	0.9996
10.0	0.9982	0.9982	0.9982	0.9983	0.9984	0.9984	0.9984	0.9985	0.9984
20.0	0.9975	0.9974	0.9974	0.9975	0.9976	0.9977	0.9977	0.9977	0.9977
100	0.9971	0.9974	0.9974	0.9975	0.9976	0.9977	0.9977	0.9977	0.9977

6. Conclusions

In this study, the concept of EMR is developed for vibration analysis of cracked piezoelectric functionally graded beams. First, mechanical frequency response of cracked functionally graded beams bonded with a piezoelectric layer under a concentrated load was conducted and used for calculating electric charge produced in the piezoelectric layer. Next, from the electrical charge acknowledged as electrical response, the EMR of the integrated FGM beams has been analytically derived and numerically examined in the frequency domain surrounding the beam's fundamental frequency. It was proved again herein that the electrical response obtained totally in the piezoelectric layer is spectrally similar to the mechanical response measured at the beam's middle. This fact strongly authorizes the reliability of using the piezoelectric layer as a distributed sensor for measurement of the beam's dynamic deflection. Finally, a spectral damage index defined by the coherence coefficient between EMRs of cracked and intact beams and acknowledged as EMR sensitivity to crack is numerically examined along with not only crack parameters but also material gradient index and position of load application. It was found that the introduced spectral damage index is sensitive to crack much more than the conventional frequency response functions and provides a novel useful indicator for crack detection in FGM beams by piezoelectric sensors.

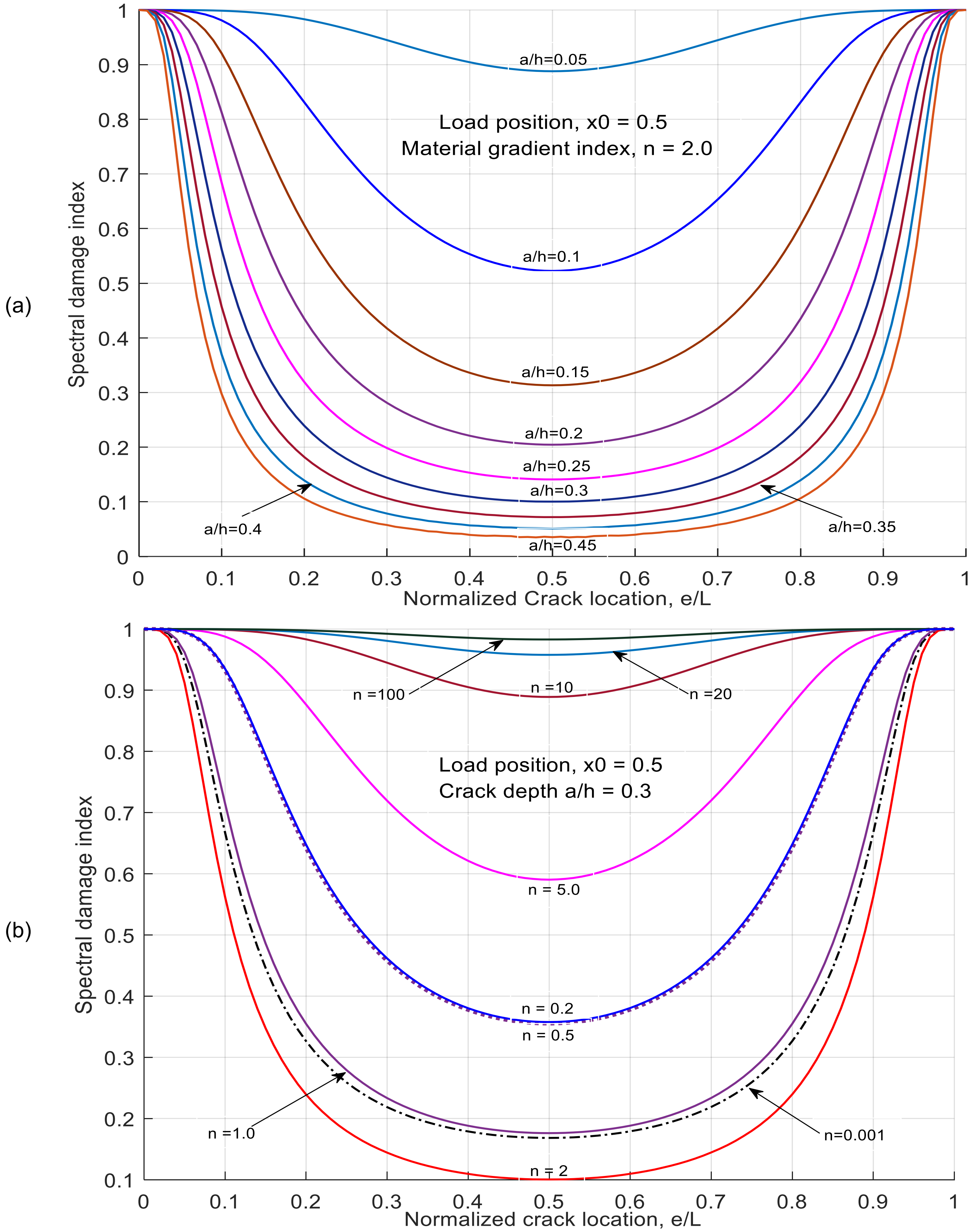

Fig. 5. Spectral damage index versus crack location in various crack depth (a) and material grading index (b) in case of load applied at the beam midspan (x_0 = L/2).

(a)

(b)

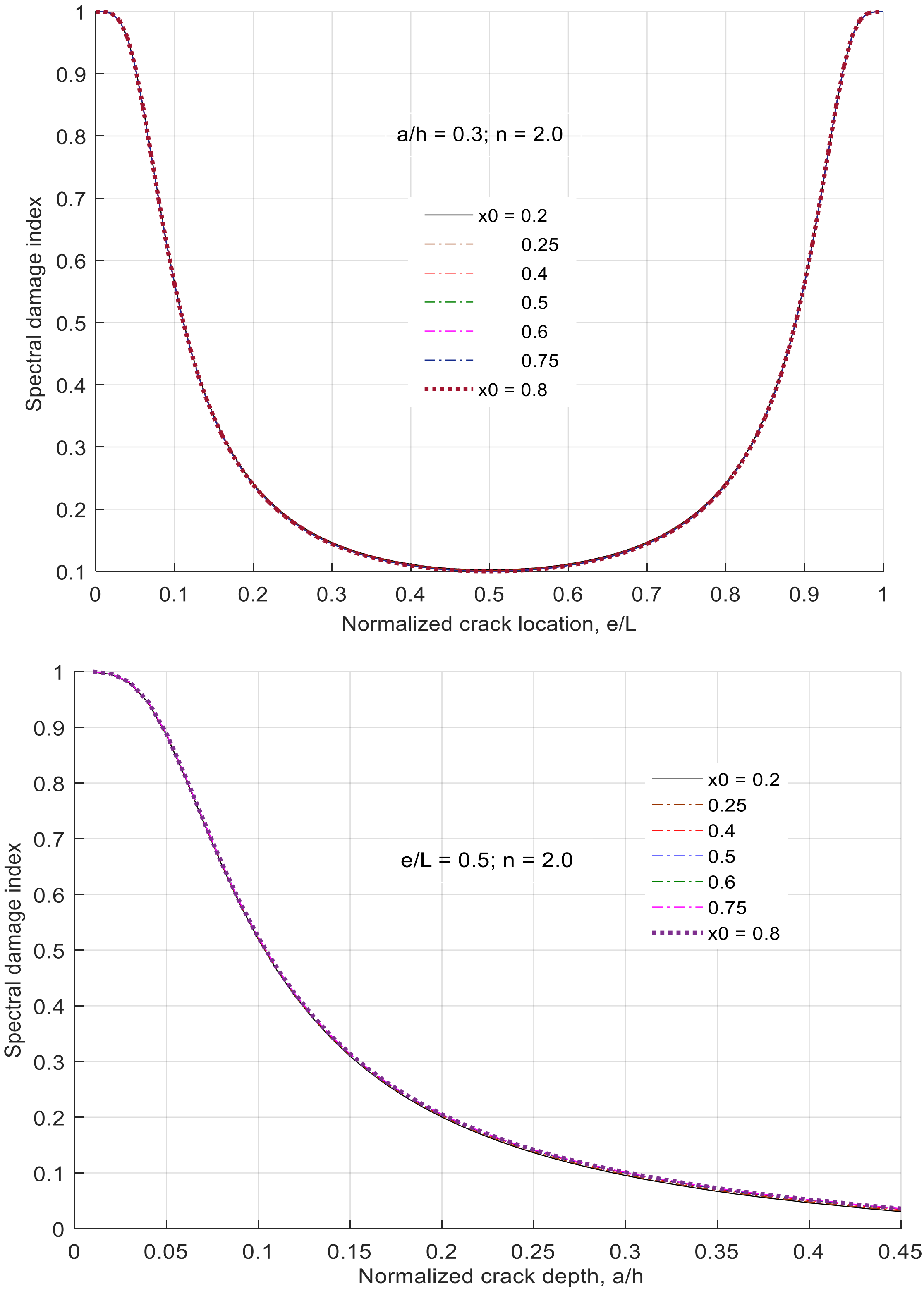

Fig. 6. Spectral damage index versus crack location (a) and crack depth (b) in various positions of load application x_0.

Acknowledgments

This research was funded by Thuyloi University under Project number CS2025-04. The author sincerely thanks Thuyloi University for funding the implementation of the project.

Declaration of Generative AI

During the preparation of this work, the authors do not use Generative AI and AI-assisted technologies tools in order to generate the content of the manuscript.

References

[1]. V. Birman, L.W. Byrd. (2007). Modeling and Analysis of Functional Graded Materials and Structures. *Applied Mechanics Reviews*, 60(5), 195-215. https://doi.org/10.1115/1.2777164

[2]. A. Gupta, M. Talha. (2015). Recent development in modeling and analysis of functionally graded materials and structures. *Progress in Aerospace Sciences*, 79, 1-14. https://doi.org/10.1016/j.paerosci.2015.07.001

[3]. P. Sharma. (2021). Vibration analysis of FGPM beam: A review. *Material Today: Proceeding*, 44(Part 1), 1384-1390. https://doi.org/10.1016/j.matpr.2020.11.621

[4]. R. Singh, P. Sharma. (2019). A Review on Modal Characteristics of FGM Structures. *AIP Conference Proceedings*, 2148(1), 030037. https://doi.org/10.1063/1.5123959

[5]. P. Zahedinejad, C. Zhang, H. Zhang, S. Ju. (2020). A Comprehensive Review on Vibration Analysis of Functionally Graded Beams. *International Journal of Structural Stability and Dynamics*, 20(04), 2030002. https://doi.org/10.1142/S0219455420300025

[6]. D. Gayen, R. Tiwari, D. Chakraborty. (2019). Static and Dynamic Analysis of Cracked Functionally Graded Structural Components: A Review. *Composite Part B: Engineering*, 173, 106982. https://doi.org/10.1016/j.compositesb.2019.106982

[7]. G.P. Sinha, B. Kumar. (2021). Review on Vibration Analysis of Functionally Graded Material Structural Components with Cracks. *Journal of Vibration Engineering & Technologies*, 9(1), 23-49. https://doi.org/10.1007/s42417-020-00208-3

[8]. N.T. Khiem. (2022). Vibration of Cracked Functionally Graded Beams: General Solution and Application – A Review. *Vietnam Journal of Mechanics*, 44(4), 317-347. https://doi.org/10.15625/0866-7136/17986

[9]. A. Banerjee, B. Panigrahi, G. Pohit. (2016). Crack modelling and detection in Timoshenko FGM beam under transverse vibration using frequency contour and response surface model with GA. *Nondestructive Testing and Evaluation*, 31(2), 142-164. https://doi.org/10.1080/10589759.2015.1071812

[10]. N.T. Khiem, N.N. Huyen. (2017). A method for crack identification in functionally graded Timoshenko beam. *Nondestructive Testing and Evaluation*, 32(3), 319-341. https://doi.org/10.1080/10589759.2016.1226304

[11]. Z.G. Yu, F.L. Chu. (2009). Identification of crack in functionally graded material beams using the p-version of finite element method. *Journal of Sound and Vibration*, 325(1-2), 69-84. https://doi.org/10.1016/j.jsv.2009.03.010

[12]. N.T. Khiem, T.H. Hai, L.Q. Huong. (2023) Crack identification for functionally graded beam using distributed piezoelectric sensor. *Journal of Vibration and Control*, 29(15-16), 3401-3417. https://doi.org/10.1177/10775463221095649

[13]. S.S. Rao, M. Sunar. (1994). Piezoelectricity and its use in disturbance sensing and control of flexible structures: A survey. *Applied Mechanics Reviews*, 47(4), 113-123. https://doi.org/10.1115/1.3111074

[14]. G. Huang, F. Song, X. Wang. (2010). Quantitative modeling of coupled piezo-elastodynamic behavior of piezoelectric actuators bonded to an elastic medium for structural health monitoring: a review. *Sensor*, 10(4), 3681-3702. https://doi.org/10.3390/s100403681

[15]. G. Park, H. Sohn, C. R. Farrar, D. J. Inman. (2003). Overview of piezoelectric impedance-based health monitoring and path forward. *The Shock and Vibration Digest*, 35(6), 451-464. https://doi.org/10.1177/05831024030356001

[16]. G. Song, H. Gu, H. Li. (2012). Application of the piezoelectric material for health monitoring

in civil engineering: an overview. *ASCE Proceedings: Engineering, Construction, and Operations in Challenging Environments: Earth and Space 2004, pp. 680-687.* https://doi.org/10.1061/40722(153)94

[17]. V.G.M. Annamdas, C.K. Soh. (2010). Application of electromechanical impedance technique for engineering structures: review and future issues. *Journal of Intelligent Material Systems and Structures*, 21(1), 41-59. https://doi.org/10.1177/1045389X09352816

[18]. K.K. Maurya, A. Rawat, G. Jha. (2020). Smart material and electromechanical impedance technique: a review. *Materials Today: Proceedings*, 33(Part 8), 4993-5000. https://doi.org/10.1016/j.matpr.2020.02.831

[19]. W.S. Na, J. Baek. (2018). A review of the piezoelectric electromechanical impedance based structural health monitoring technique for engineering structures. *Sensor*, 18(5), 1307. https://doi.org/10.3390/s18051307

[20]. S. Park, S. Ahmad, C.B. Yun, Y. Roh. (2006). Multiple crack detection of concrete structures using impedance-based structural health monitoring techniques. *Experimental Mechanics*, 46(5), 609-618. https://doi.org/10.1007/s11340-006-8734-0

[21]. D. Wang, H. Song, H. Zhu. (2015). Electromechanical impedance analysis on piezoelectric smart beam with a crack based on spectral element method. *Mathematical Problems in Engineering*, 2015, 713501. https://doi.org/10.1155/2015/713501

[22]. T. Wang, B. Tan, M. Lu, Z. Zhang, G. Lu. (2020). Piezoelectric Electro-mechanical impedance (EMI) based structural crack monitoring. *Applied Sciences*, 10(13), 4648. https://doi.org/10.3390/app10134648

[23]. W. Yan, J.B. Cai, W.Q. Chen. (2011). An electro-mechanical impedance model of a cracked composite beam with adhesively bonded piezoelectric patches. *Journal of Sound and Vibration*, 330(2), 287-307. https://doi.org/10.1016/j.jsv.2010.08.013

[24]. W. Yan, W.Q. Chen, C.W. Lim, J.B. Cai. (2008). Application of EMI technique for crack detection in continuous beams adhesively bonded with multiple piezoelectric patches. *Mechanics of Advanced Materials and Structures*, 15(1), 1-11. https://doi.org/10.1080/15376490701410513

[25]. G. Roy, B. Panigrahi, G. Pohit. (2021). Crack identification in beam-type structural elements using piezoelectric sensor. *Nondestructive Testing and Evaluation*, 36(6), 597-615. https://doi.org/10.1080/10589759.2020.1843652

[26]. P.S. Sumant, S.K. Maiti. (2006). Crack detection in a beam using PZT sensor. *Smart Materials and Structures*, 15(3), 695-703. https://doi.org/10.1088/0964-1726/15/3/004

[27]. T.T. Hai, P.T. Hang, N.T. Khiem. (2024). A novel criterion for crack identification in beam-like structures using distributed piezoelectric sensor and controlled moving load. *Journal of Sound and Vibration*, 572, 118155. https://doi.org/10.1016/j.jsv.2023.118155

[28]. T.T. Hai, L.K. Toan, N.N. Huyen, N.T. Khiem. (2025). Electro-Mechanical Receptance Concept for Cracked Piezoelectric Timoshenko Beams and Application. *Journal of Vibration Engineering & Technologies*, 13(1), 90. https://doi.org/10.1007/s42417-024-01635-2